Kinetic Simulation of Unsteady Detonation with Nonequilibrium Effects

Lin C.[1], Luo K.[2,*]

[1] *Tsinghua University, Beijing, China*
[2] *University College London, London, UK*
**Corresponding author's email: K.Luo@ucl.ac.uk*

ABSTRACT

A discrete Boltzmann method (DBM) is proposed for simulating unsteady detonation with nonequilibrium effects. The chemical reaction is naturally coupled with the fluid flow via the reaction term. The chemical reaction is expressed by a two-step reaction scheme. Both the discrete equilibrium distribution function and the chemical term in the velocity space are transformed from the kinetic space with a matrix inversion method. The DBM could recover the reactive Navier-Stokes equations in the hydrodynamic limit, while it has the capability of measuring detailed thermodynamic non-equilibrium effects. Moreover, this model is employed to study the dynamic process of the unsteady non-equilibrium detonation. The reaction zone, transverse shock wave, leading shock front, Mach stem, and triple point are clearly captured by using non-equilibrium manifestations. In addition, the non-equilibrium effect is stronger for larger chemical heat release. It displays periodic oscillations as the time goes on. Its oscillation amplitude decreases with decreasing chemical heat release, and approaches zero when the chemical heat is small enough. The transverse wave and cellular pattern exist for large chemical heat, but disappear for small chemical heat release.

KEYWORDS: Discrete Boltzmann, lattice Boltzmann, unsteady detonation, non-equilibrium effect.

INTRODUCTION

Detonation is a type of shock-induced combustion where the exothermic energy release contributes to sustaining the shock. A detonation wave can be seen as a shock wave coupled with a reaction zone [1]. Detonation phenomena are widely studied due to their importance to engineering and safety. In the fields of mining, gas explosion, hazardous materials transportation, for example, the study of detonation is aimed at the prevention or control of destruction [2, 3]. In the meantime, detonation has numerous industrial and engineering applications [4, 5], such as accelerating projectiles, cleaning equipment, coating a surface, etc.

In general, detonation is in a dynamic process where chemical reactions and fluid flow interact with each other, leading to both hydrodynamic and thermodynamic nonequilibrium behaviours [6, 7]. Traditional simulation methods are based on Euler or Navier-Stokes (NS) solvers. Compared with the Euler model, the NS model contains the diffusion and heat conduction that often can not be neglected [8]. However, NS methods also neglect various nonequilibrium effects which usually play essential roles in detonation. Such a method can be problematic [6, 7], as hydrodynamic solvers often prove to be inadequate for non-equilibrium reacting systems which evolve over several orders of spatio-temporal scales.

For an accurate description of unsteady detonation with nonequilibrium effects, it is feasible to resort to the Boltzmann equation, which is a fundamental equation in kinetic theory. Roughly

Proceedings of the Ninth International Seminar on Fire and Explosion Hazards (ISFEH9), pp. 289-300
Edited by Snegirev A., Liu N.A., Tamanini F., Bradley D., Molkov V., and Chaumeix N.
Published by St. Petersburg Polytechnic University Press
ISBN: 978-5-7422-6496-5 DOI: 10.18720/spbpu/2/k19-113

speaking, there are two categories of methods to obtain solutions of the Boltzmann equation. One is stochastic simulation, such as the well known direct simulation Monte Carlo [9]. The main drawbacks include the slow numerical convergence and random fluctuations. The other is deterministic techniques, such as the lattice Boltzmann method (LBM) [10], the discrete unified gas-kinetic scheme [11], discrete Boltzmann method (DBM) [12], etc.

As a novel kinetic method, the recently developed DBM is regarded as a variant developed from the standard LBM. Most standard LBMs for reacting flows are confined to incompressible low-speed systems [13]-[16]. The pioneering LBM for combustion was developed in the limit of fast chemistry [13]. The first DBM for combustion and detonation was proposed and utilized to probe thermodynamic nonequilibrium effects around the detonation wave [17]. Actually, the DBM has several advantages over the standard LBM. (I) With enough kinetic moment relations satisfied, the DBM could recover the full NS equations, instead of incompressible NS equations, in the hydrodynamic limit. (II) The expression of discrete equilibrium distribution function is obtained from the its kinetic moment relations, without the restriction that the flow speed is small. (III) The time step, space step and discrete velocities are decoupled in the DBM, their flexible values could be adjusted to improve the robustness and accuracy of numerical simulation.

The DBM has the capability of simulating both subsonic and supersonic combustion in a physically accurate way. However, previous DBM works were mainly focused on steady combustion and detonation [18-20]. In this work, we further develop and employ the DBM to investigate the unsteady nonequilibrium detonation. The dynamic process of the detonation wave is analysed and discussed. The application of DBM to detonation phenomena not only allows a deeper understanding of physical mechanisms in the ubiquitous non-equilibrium reactive flows, but also provides valuable reference data for traditional models to compare.

KINETIC MODEL

The present kinetic model is based on the discrete Boltzmann equation as below,

$$\partial_t f_i + \mathbf{v}_i \cdot \nabla f_i = \Omega_i + R_i , \tag{1}$$

where $\partial_t f_i$ is the partial derivative of the discrete distribution function f_i with respect to the time t, $\mathbf{v}_i$ denotes the discrete velocity with the subscript i = 1, 2, … , 16. To be specific,

$$\mathbf{v}_i = \begin{cases} \text{cyc}:(\pm v_a, 0) & i = 1 \sim 4, \\ \text{cyc}:(\pm v_b, \pm v_b) & i = 5 \sim 8, \\ \text{cyc}:(\pm v_c, 0) & i = 9 \sim 12, \\ \text{cyc}:(\pm v_d, \pm v_d) & i = 13 \sim 16, \end{cases} \tag{2}$$

where cyc denotes the cyclic permutation, v_a, v_b, v_c, and v_d are adjustable parameters, see Fig. 1.

The collision term, as a discretization of the Bhatnagar-Gross-Krook (BGK) model, takes the following form

$$\Omega_i = \frac{1}{\tau}\left(f_i - f_i^{eq} \right), \tag{3}$$

where τ is the relaxation time, f_i^{eq} is the discrete equilibrium distribution function. To recover the NS equations, f_i^{eq} is required to satisfy the following relations,

$$\int\int f^{eq} d\mathbf{v} d\eta = \rho = \sum_i f_i^{eq} , \tag{4}$$

$$\int\int f^{eq} v_\alpha d\mathbf{v} d\eta = \rho u_\alpha = \sum_i f_i^{eq} v_{i\alpha} , \tag{5}$$

$$\int\int f^{eq} \left(v^2 + \eta^2\right) d\mathbf{v} d\eta = \rho\left[(D+I)T + u^2\right] = \sum_i f_i^{eq} \left(v_i^2 + \eta_i^2\right), \tag{6}$$

$$\int\int f^{eq} v_\alpha v_\beta d\mathbf{v} d\eta = \rho\left(\delta_{\alpha\beta} T + u_\alpha u_\beta\right) = \sum_i f_i^{eq} v_{i\alpha} v_{i\beta} , \tag{7}$$

$$\int\int f^{eq} \left(v^2 + \eta^2\right) v_\alpha d\mathbf{v} d\eta = \rho u_\alpha \left[(D+I+2)T + u^2\right] = \sum_i f_i^{eq} \left(v_i^2 + \eta_i^2\right) v_{i\alpha} , \tag{8}$$

$$\int\int f^{eq} v_\alpha v_\beta v_\chi d\mathbf{v} d\eta = \rho\left(u_\alpha \delta_{\beta\chi} + u_\beta \delta_{\alpha\chi} + u_\chi \delta_{\alpha\beta}\right) T + \rho u_\alpha u_\beta u_\chi = \sum_i f_i^{eq} v_{i\alpha} v_{i\beta} v_{i\chi} , \tag{9}$$

$$\begin{aligned} &\int\int f^{eq} \left(v^2 + \eta^2\right) v_\alpha v_\beta d\mathbf{v} d\eta = \rho\delta_{\alpha\beta}\left[(D+I+2)T + u^2\right] T + \rho u_\alpha u_\beta \left[(D+I+4)T + u^2\right], \\ &= \sum_i f_i^{eq} \left(v_i^2 + \eta_i^2\right) v_{i\alpha} v_{i\beta} \end{aligned} \tag{10}$$

where ρ is the density, u_α the velocity in the α direction, T temperature, $D = 2$ the dimension, I the extra degrees of freedom, and

$$\eta_i = \begin{cases} \eta_a & i = 1 \sim 4, \\ \eta_b & i = 5 \sim 8, \\ \eta_c & i = 9 \sim 12, \\ \eta_d & i = 13 \sim 16, \end{cases} \tag{11}$$

with adjustable parameters η_a, η_b, η_c, and η_d. It is worth mentioning that the parameters (v_a, v_b, v_c, v_d, η_a, η_b, η_c, η_d) could be adjusted to optimize the properties of the DBM. (i) The values of v_a, v_b, v_c, and v_d are chosen by reference to flow velocity $\mathbf{u}$, sound speed $v_s = \sqrt{\gamma T}$, and shock speed, etc. (ii) The values of η_a, η_b, η_c, and η_d are relative to $\sqrt{IT}$.

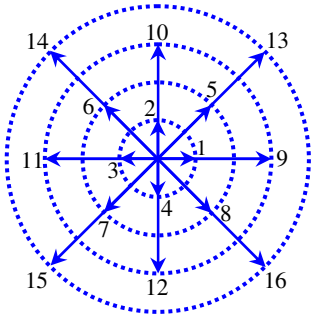

Fig. 1. Schematic of the discrete velocity model.

According to the equipartition of energy theorem, $m\overline{\eta}^2/2 = IT/2$ for an equilibrium system, where $m = 1$ is the particle mass, $\overline{\eta}^2$ represents the average value of η^2. Moreover, the specific heat ratio, $\gamma = (D+I+2)/(D+I)$, is flexible as the parameter I is adjustable. Actually, Eqs. (4)-(10) can be uniformly written as

$$\mathbf{M}_{\mathbf{f}}^{eq} = \mathbf{C}\mathbf{f}^{eq}, \tag{12}$$

where $\mathbf{f}^{eq} = \left(f_1^{eq}, f_2^{eq}, \cdots, f_{16}^{eq}\right)^{\mathrm{T}}$ is the set of discrete equilibrium distribution functions, $\mathbf{M}_{\mathbf{f}}^{eq} = \left(M_{f1}^{eq}, M_{f2}^{eq}, \cdots, M_{f16}^{eq}\right)^{\mathrm{T}}$ is the set of kinetic moment, and $\mathbf{C}$ is a square matrix linking the velocity space to moment space, see APPENDIX. Hence, the discrete distribution function is obtained as below

$$\mathbf{f}^{eq} = \mathbf{C}^{-1}\mathbf{M}_{\mathbf{f}}^{eq}. \tag{13}$$

Similarly, the reaction term R_i is required to satisfy the following relations,

$$\int\int R d\mathbf{v} d\eta = 0 = \sum\nolimits_i R_i, \tag{14}$$

$$\int\int R v_\alpha d\mathbf{v} d\eta = 0 = \sum\nolimits_i R_i v_{i\alpha}, \tag{15}$$

$$\int\int R\left(v^2+\eta^2\right) d\mathbf{v} d\eta = \rho(D+I)T = \sum\nolimits_i R_i\left(v_i^2+\eta_i^2\right), \tag{16}$$

$$\int\int R v_\alpha v_\beta d\mathbf{v} d\eta = \delta_{\alpha\beta}\rho T' = \sum\nolimits_i R_i v_{i\alpha} v_{i\beta}, \tag{17}$$

$$\int\int R\left(v^2+\eta^2\right) v_\alpha d\mathbf{v} d\eta = (D+I+2)\rho u_\alpha T' = \sum\nolimits_i R_i\left(v_i^2+\eta_i^2\right) v_{i\alpha}, \tag{18}$$

$$\int\int R v_\alpha v_\beta v_\chi d\mathbf{v} d\eta = \rho\left(u_\alpha\delta_{\beta\chi} + u_\beta\delta_{\alpha\chi} + u_\chi\delta_{\alpha\beta}\right)T' = \sum\nolimits_i R_i v_{i\alpha} v_{i\beta} v_{i\chi}, \tag{19}$$

$$\begin{aligned}&\int\int R\left(v^2+\eta^2\right) v_\alpha v_\beta d\mathbf{v} d\eta = \rho\left[2T(D+I+2)\delta_{\alpha\beta} + (D+I+5)u_\alpha u_\beta + u^2\right]T' \\ &= \sum\nolimits_i R_i\left(v_i^2+\eta_i^2\right) v_{i\alpha} v_{i\beta}\end{aligned}, \tag{20}$$

which can be expressed in a uniform formula,

$$\mathbf{M}_{\mathbf{R}} = \mathbf{C}\mathbf{R}, \tag{21}$$

see APPENDIX for details. Consequently, the reaction term is specified as

$$\mathbf{R} = \mathbf{C}^{-1}\mathbf{M}_{\mathbf{R}}. \tag{22}$$

It is clear that the reaction term depends upon not only (ρ, u_α, T, D, I), but also the change rate of temperature due to the chemical reaction,

$$T' = \frac{2Q\lambda'}{D+I}, \tag{23}$$

where Q is the chemical heat release per unit mass of the chemical reactant, λ' is the change rate of the reaction progress λ. In this work, we employ the following two-step reaction function [21],

$$\xi' = Hk_I \exp\left[E_I\left(T_s^{-1} - T^{-1}\right)\right], \tag{24}$$

$$\lambda' = (1-H)k_R(1-\lambda)\exp\left(-E_R T^{-1}\right), \tag{25}$$

where $H=1$ for $\xi<1$, and $H=0$ for $\xi\geq 1$. ξ represents the reaction progress variable within a thermally neutral induction zone, and λ denotes the reaction progress variable within an

exothermic reaction zone. Here λ is defined as the mass fraction of the product. k_I and E_I are the rate constant and activation energy for the ignition process, respectively. k_R and E_R are the rate constant and activation energy for the reaction process, respectively. T_s stands for the temperature behind the pre-shock wave.

It is easy to prove that the DBM could recover the reactive NS equations in the hydrodynamic limit. Moreover, it contains various detailed nonequilibrium manifestations beyond the NS equations. To be specific, we can obtain the following nonequilibrium manifestations

$$\mathbf{M}_{\mathbf{f}}^{neq}=\mathbf{M}_{\mathbf{f}}-\mathbf{M}_{\mathbf{f}}^{eq}, \tag{26}$$

in each iterative step, with $\mathbf{M}_{\mathbf{f}}^{neq}=\left(M_{f1}^{neq},M_{f2}^{neq},\cdots,M_{f16}^{neq}\right)^{\mathrm{T}}$ and $M_{fi}^{neq}=M_{fi}-M_{fi}^{eq}$. To have a general quantitative measure of nonequilibrium, we introduce the non-equilibrium intensity,

$$\Delta=\sqrt{\sum_{i=1}^{16}M_{fi}^{neq}}=\sqrt{\sum_{i=5}^{16}M_{fi}^{neq}}, \tag{27}$$

since $M_{f1}^{neq}=M_{f2}^{neq}=M_{f3}^{neq}=M_{f4}^{neq}=0$ in accordance with the conservation of mass, momentum, and energy, respectively. The non-equilibrium degree is the distance in the kinetic-moment space of the nonequilibrium part of the distribution function.

SIMULATION RESULTS

In this section, we firstly validate the DBM model with three benchmarks, i.e., the Colella explosion wave, exothermic chemical reaction, and steady detonation. Then we employ the present model to investigate the unsteady detonation with nonequilibrium effects. Furthermore, the second order Runge-Kutta scheme and the second order non-oscillatory and nonfree-parameter dissipation difference scheme [22] are chosen to solve Eq. (1). The inflow and outflow boundary conditions are utilized in the x direction, and the periodic boundary condition is adopted in the y direction. All physical quantities are written in nondimensional forms, namely, the widely used LB units [20].

Colella explosion wave

The shock tube problem is a common test for the robustness and accuracy of a numerical method. As a typical Riemann problem, the Colella explosion wave is simulated here. Colella explosion problem was originally employed by Woodward and Colella to test several hydrodynamic methods for systems involving strong shocks and narrow features [23]. Generally, this case is regarded as a challenging test. On the one hand, it contains extremely large pressure and temperature ratios, up to 100,000. On the other, there is simultaneously a leftward rarefaction wave, a contact discontinuity, and a rightward shock front, see Fig.2 (a).

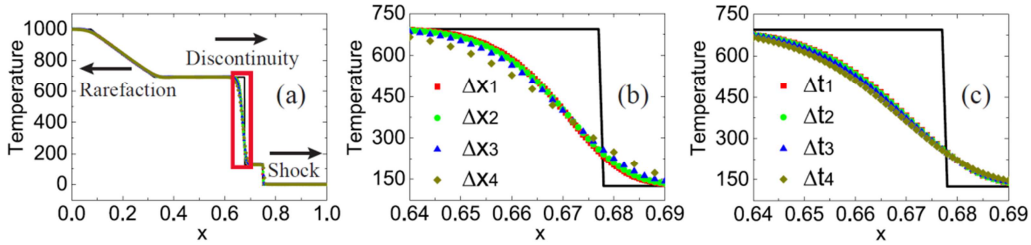

Fig. 2. Temperature profile around the Celella explosion wave.

The initial field reads

$$\begin{cases} \left(\rho, u_x, u_y, T\right)_L = (1,0,0,1000) \\ \left(\rho, u_x, u_y, T\right)_R = (1,0,0,0.01) \end{cases},$$

where the subscript L indicates $0 \le x < 0.5$, and R indicates $0.5 \le x \le 1$. The relaxation time $\tau = 2\times10^{-5}$, the specific heat ratio $\gamma = 1.8$, the parameters (v_a, v_b, v_c, v_d, η_a, η_b, η_c, η_d) = (42, 37, 32, 12, 27, 0, 0, 10).

Figure 2 delineates the temperature profile around the Celella explosion wave at a time instant $t = 0.01$. To perform a study of the solution to the grid size and the time step, the simulation is conducted with various space and time steps, respectively. Panel (b) corresponds to the amplified area labelled by the rectangle in panel (a). In panels (a) and (b), the line denotes the theoretical results, the squares, circles, triangles, and diamonds, represent the DBM results with fixed time step $\Delta t = 5\times10^{-5}$, and various space steps, $\Delta x_1 = 5\times10^{-4}$, $\Delta x_2 = 10^{-3}$, $\Delta x_3 = 2\times10^{-3}$, and $\Delta x_4 = 4\times10^{-3}$, respectively. Similarly, panel (c) gives the DBM results with fixed space step $\Delta x = \Delta y = 10^{-3}$, and various time steps, $\Delta t_1 = 1.25\times10^{-6}$, $\Delta t_2 = 2.5\times10^{-6}$, $\Delta t_3 = 5\times10^{-6}$, and $\Delta t_4 = 10^{-5}$, respectively. It can be found in panels (b) and (c) that with decreasing space or time steps, the numerical error becomes smaller and smaller. In addition, there are some differences between the DBM results and the theoretical solutions, because the theoretical solutions ignore the physical viscosity and heat conduction. In contrast, the DBM takes account of the viscosity, heat conduction and various thermodynamic non-equilibrium processes.

EXOTHERMIC CHEMICAL REACTION

For the sake of validating the effect of the chemical reaction on the flow field, we simulate the exothermic chemical reaction. The configuration is as follows: in a closed box, the chemical reactant is distributed evenly with the initial density $\rho_0 = 1$, temperature $T_0 = 1$, and velocity $\mathbf{u} = 0$, respectively. The chemical reaction takes place with parameters (k_I, E_I, k_R, E_R) = (5000, 8, 10000, 1). During the reaction process, the chemical heat is transformed into the internal energy and/or kinetic energy. Theoretically, the temperature becomes $T = T_0 + (\gamma - 1)Q$ after chemical reaction. The period boundary condition is imposed in each direction. The relaxation time is $\tau = 5\times10^{-6}$, the grid $N_x = N_y = 1$, the space step $\Delta x = \Delta y = 2\times10^{-5}$, the time step $\Delta t = 10^{-6}$, and the parameters (v_a, v_b, v_c, v_d, η_a, η_b, η_c, η_d) = (4, 3.6, 2.2, 0.7, 0, 0, 0, 2.6).

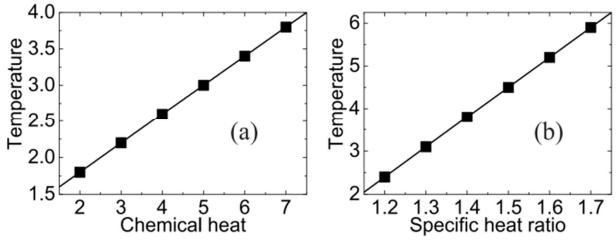

Fig. 3. Temperature after the exothermic chemical reaction: (a) with various chemical heat release, (b) with various specific heat ratios.

Figure 3 illustrates the temperature after chemical reaction with various chemical heat release (a) and specific heat ratios (b). The squares represent the DBM results, and the lines represent the theoretical solutions. Panel (a) shows that the temperature of the chemical product increases linearly with the increasing chemical heat release. Panel (b) demonstrates the linear relation between the temperature and the specific heat ratio. We also find a perfect agreement between the two sets of results in panels (a) and (b), respectively. Our DBM results are exactly equal to the theoretical solutions with various chemical heat release and specific heat ratios. Consequently, it is confirmed that the chemical energy is naturally converted into heat energy via the reaction term in the discrete Boltzmann equation.

STEADY DETONATION

For the purpose of validating the DBM suitable for supersonic reactive flows, we carry out the simulation of a 1-D steady detonation. The detonation wave travels from left to right, with the chemical heat release $Q=2$. The initial field, which satisfies the Rankine-Hugoniot relation, takes the following form [24],

$$\begin{cases}\left(\rho,u_x,u_y,T,\xi,\lambda\right)_L=\left(1.48043,0.81650,0,2.06314,1,1\right)\\ \left(\rho,u_x,u_y,T,\xi,\lambda\right)_R=\left(1,0,0,1,0,0\right)\end{cases},$$

where the subscript L indicates $0\le x<0.01$, and R indicates $0.01\le x\le 0.1$. The left part is occupied by the chemical product, and the right part is filled with the chemical reactant. As the detonation propagates forwards, chemical reaction takes place violently around the detonation wave, and the pressure increases sharply. The relaxation time $\tau=5\times10^{-6}$, the specific heat ratio $\gamma=1.4$, the parameters (k_I, E_I, k_R, E_R) = (5000, 8, 2000, 1), (v_a, v_b, v_c, v_d, η_a, η_b, η_c, η_d) = (4, 3.6, 2.2, 0.7, 0, 0, 0, 2.6).

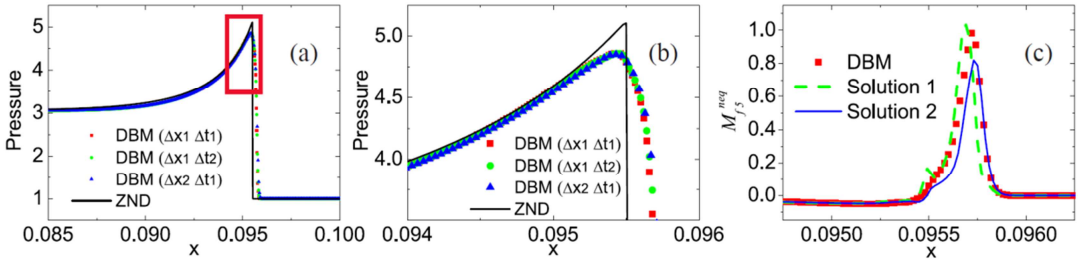

Fig. 4. The pressure p and the nonequilibrium quantity M_{f5}^{neq} around the steady detonation wave.

Figure 4 (a) displays the pressure profile at a time instant $t=0.036$. The squares denote the DBM with space and time steps, (Δx_1, Δt_1) = (2×10^{-5}, 10^{-6}), the circles denote (Δx_1, Δt_2) = (2×10^{-5}, 2×10^{-6}), the triangles denote (Δx_2, Δt_1) = (4×10^{-5}, 10^{-6}). The line stands for the ZND (named after Zel'dovich, von Neumann, and Döring) solution [24]. Figure 4 (b) corresponds to the amplified area labelled by the rectangle in Fig. 4 (a). It is clear that the DBM results with the three different space and time steps are close to each other. For the case with (Δx_1, Δt_1), the simulation pressure behind the detonation wave is 3.05317. Compared with the analytic value 3.05433, the relative error is 0.04%. Moreover, the simulation detonation speed is 2.508, the relative error is 0.32% in comparison with the theoretical result 2.516. Clearly, the results are satisfactory.

Moreover, there are some differences between the DBM and ZND results around the detonation peak. Because the ZND assumes that the detonation structure consists of an infinitely thin leading shock that compresses the reactant gas to high pressure and temperature, viscosity and heat conduction are neglected. In contrast, the DBM takes into account of the viscosity and heat conduction, which smooth and reduce the shock wave.

To demonstrate the ability to resolve non-equilibrium effects, Fig. 4 (c) illustrates the non-equilibrium quantity M_{f5}^{neq} around the detonation wave. The symbols stand for the DBM results, the solid line is for the solution in Ref. [12], and the dashed line is for the solution in Ref. [19]. Both solutions are derived from the first-order truncation of distribution function in different ways. There are a few differences between our DBM results and the two solutions. Theoretically, the first-order truncation of distribution function corresponds to the NS equations. And the current DBM is actually more accurate than the solutions at the first-order level.

Unsteady detonation

Next, let us simulate and study unsteady detonation. The computational domain is chosen as $L_x \times L_y = 0.01 \times 0.03$, and the other parameters are the same as those in Fig. 4. In order to trigger the instability, a perturbation is imposed on the initial field, i.e.,

$$\rho = \frac{\rho_L + \rho_R}{2} - \frac{\rho_L - \rho_R}{2}\tanh\left(\frac{x - x_0}{W}\right),\ T = \frac{T_L + T_R}{2} - \frac{T_L - T_R}{2}\tanh\left(\frac{x - x_0}{W}\right),$$

$$\mathbf{u} = \frac{\mathbf{u}_L + \mathbf{u}_R}{2} - \frac{\mathbf{u}_L - \mathbf{u}_R}{2}\tanh\left(\frac{x - x_0}{W}\right),\ \lambda = \frac{\lambda_L + \lambda_R}{2} - \frac{\lambda_L - \lambda_R}{2}\tanh\left(\frac{x - x_0}{W}\right),$$

where the initial configuration is divided into two parts along a curve, see Fig. 5. The physical quantities are $(\rho_L,\ T_L,\ \mathbf{u}_L,\ \lambda_L) = (1.48043,\ 2.06314,\ -1.69953\mathbf{e}_x,\ 1)$ on the left side, and $(\rho_R,\ T_R,\ \mathbf{u}_R,\ \lambda_R) = (1,\ 1,\ -2.51603\mathbf{e}_x,\ 0)$ on the right side. The left part is full of the chemical product, and the right part is for the chemical reactant. $W = L_y/50$ is the layer width across the interface between the two parts.

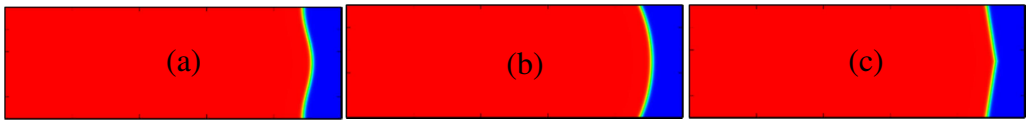

Fig. 5. Initial configurations of the unsteady detonation with various shapes of perturbation: (a) sine, (b) circular arc, (c) triangle.

Figure 5 illustrates the initial configurations of the unsteady detonation with various shapes of perturbation. Figure 5 (a) is implosed on with a sine curve,

$$x_0 = L_x/10 - A_0\cos(ky),$$

with an amplitude $A_0 = 2\times10^{-4}$ and wave number $k = 2\pi/L_y$. Figure 5 (b) is for a circular arc,

$$x_0 = \frac{L_x}{2} + \sqrt{\left(\frac{2L_x}{5}\right)^2 + \left(\frac{L_y}{4}\right)^2 - \left(y - \frac{L_y}{2}\right)^2}\ .$$

Figure 5 (c) is for a triangle,

$$x_0 = \begin{cases} \dfrac{9L_x}{10} + \dfrac{4y_0 - L_y}{25}, \text{ for } 0 < y_0 \le \dfrac{N_y}{2} \\ \dfrac{9L_x}{10} - \dfrac{4y_0 - 3L_y}{25}, \text{ for } \dfrac{N_y}{2} < y_0 \le N_y \end{cases}.$$

Now, let us study the influence of the initial conditions on the evolution of the unsteady detonation. Figure 6 (a) illustrates the evolution of the maximum pressure. To have a clearer picture, we show the enlarged area during the early and later periods in panels (b) and (c), respectively. The solid, dashed, and dotted lines represent the sine, circular-arc, and triangle perturbations, respectively. It can be found that the maximum pressure under various initial perturbations has different amplitudes of oscillation in the early period, while it gradually attains a similar amplitude with only a phase difference in the later period. Physically, the unsteady self-sustained detonation is affected by the initial perturbation only in the early period, it gradually "forgets" the amplitude and shape of the initial perturbation and becomes self-similar with only a phase difference in the later period. Physically, once the detonation stabilizes everything left behind its sonic plane is "forgotten". This is unlike subsonic waves (i.e. flames) that tend to remember how they were perturbed.

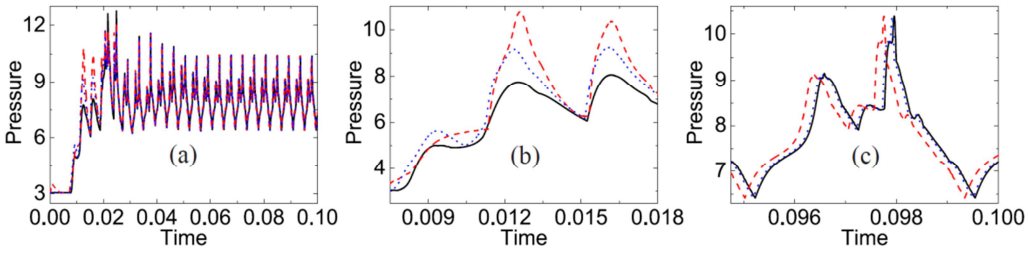

Fig. 6. Evolution of the maximum pressure. Panels (b)-(c) correspond to the enlarged area in (a).

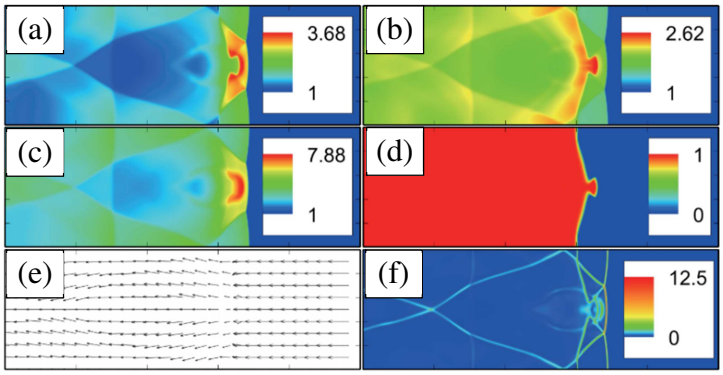

Fig. 7. Physical fields at a time instant in the detonation process: (a) density, (b) temperature, (c) pressure, (d) reaction progress variable, (e) velocity, and (f) nonequilibrium degree.

In the following, we only consider the case with the sine shape. Figure 7 depicts the contours of density, temperature, pressure, reaction progress variable, velocity, and non-equilibrium degree at time $t = 0.09$ in the evolution of the unsteady detonation. Panels (a)-(d) show that the density, temperature, and pressure increase sharply at the pre-shocked front, and then change greatly around the exothermic reaction zone. As the shock wave propagates across the chemical product and reactant, it exerts a strong influence on the flow field and chemical reaction, and the flow velocity changes simultaneously, see panel (e). In addition, it is easy to identify the pre-shock wave, the

transverse wave, the reaction zone, triple point, and the cellular structure, where the non-equilibrium degree is large, as shown in panel (f). Actually, non-equilibrium manifestations can be utilized to capture the detailed structures in the dynamic evolution of the unsteady detonation. Physically, the transverse waves collide periodically and generate high pressure and temperature. The triple point is located at the junction of the transverse wave, pre-shock front, and Mach stem. The record of the trajectories of the triple point is actually a cellular pattern.

Now, let us carry out a quantitative study on the non-equilibrium effect of the unsteady detonation. Figure 8 plots the evolution of the global nonequilibrium effect $\iint \Delta dxdy$, where the nonequilibrium intensity Δ is defined in Eq. (27), the integral is extended over the whole physical space $L_x \times L_y$. We consider four cases with various chemical heat release, i.e., $Q = 0.5$, $Q = 1.0$, $Q = 1.5$, and $Q = 2.0$. Other parameters are the same with those in Fig. 7. It is evident that the nonequilibrium effect is stronger for larger chemical heat release. It displays periodic oscillations as the time goes on. Its oscillation amplitude decreases with decreasing chemical heat release, and approaches zero when the chemical heat is small enough. Moreover, the three cases with $Q = 1.0$, $Q = 1.5$, and $Q = 2.0$ are similar with periodic evolution of transverse wave and cellular pattern. While the case with $Q = 0.5$ is significantly different from them. Figure 9 exhibits the nonequilibrium effect in the case $Q = 0.5$. It is clear that there is no transverse wave or cellular pattern for small chemical heat release.

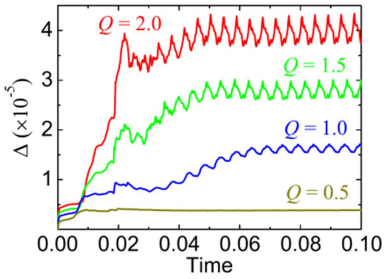

Fig. 8. The global nonequilibrium effect in the evolution of the unsteady detonation.

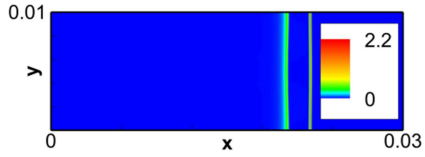

Fig. 9. The non-equilibrium effect in the unsteady detonation with small chemical heat release.

CONCLUSIONS

We present a DBM for simulating supersonic reactive flows. The chemical reaction is naturally coupled with the fluid flow via the reaction term on the right hand side of the discrete Boltzmann equation. A two-step reaction scheme is employed. Both the discrete equilibrium distribution function and the chemical term satisfying sixteen independent sets of moment relations, which are required to recover the reactive NS equations, are calculated with the matrix inversion method. Besides, the DBM has the capability of quantifying detailed thermodynamic nonequilibrium effects.

This DBM is utilized to study the unsteady nonequilibrium detonation. The reaction zone, transverse shock wave, leading shock front, Mach stem, and triple point can be clearly captured by nonequilibrium manifestations in the periodic process of the unsteady detonation. Moreover, it is demonstrated that the unsteady self-sustained detonation is affected by the initial perturbation only in the early period, starts to have similar periodic oscillations with only a phase difference in the later period. In addition, the nonequilibrium effect is stronger for larger chemical heat release. It displays periodic oscillations as the time goes on. Its oscillation amplitude decreases with

decreasing chemical heat release, and approaches zero when the chemical heat is small enough. The transverse wave and cellular pattern exist for large chemical heat, and disappear for small chemical heat release.

ACKNOWLEDGMENTS

This work is supported by the Natural Science Foundation of China (under Grant Nos. 91441120 and 51806116), the China Postdoctoral Science Foundation under Grant No. 2017M620757, and the Center for Combustion Energy at Tsinghua University. Support from the UK Engineering and Physical Sciences Research Council under the project "UK Consortium on Mesoscale Engineering Sciences (UKCOMES)" (Grant Nos. EP/L00030X/1 and EP/R029598/1) is gratefully acknowledged.

APPENDIX

The elements of $\mathbf{C}$ are

$$C_{1i}=1,\ C_{2i}=v_{ix},\ C_{3i}=v_{iy},\ C_{4i}=v_i^2+\eta_i^2,\ C_{5i}=v_{ix}^2,\ C_{6i}=v_{ix}v_{iy},\ C_{7i}=v_{iy}^2,\ C_{8i}=\left(v_i^2+\eta_i^2\right)v_{ix},$$
$$C_{9i}=\left(v_i^2+\eta_i^2\right)v_{iy},\ C_{10i}=v_{ix}^3,\ C_{11i}=v_{ix}^2v_{iy},\ C_{12i}=v_{ix}v_{iy}^2,\ C_{13i}=v_{iy}^3,\ C_{14i}=\left(v_i^2+\eta_i^2\right)v_{ix}^2,$$
$$C_{15i}=\left(v_i^2+\eta_i^2\right)v_{ix}v_{iy},\ C_{16i}=\left(v_i^2+\eta_i^2\right)v_{iy}^2.$$

The elements of $\mathbf{M}_\mathbf{f}^{eq}$ are

$$M_{f1}^{eq}=\rho,\ M_{f2}^{eq}=\rho u_x,\ M_{f3}^{eq}=\rho u_y,\ M_{f4}^{eq}=\rho\left[(D+I)T+u^2\right],\ M_{f5}^{eq}=\rho\left(T+u_x^2\right),\ M_{f6}^{eq}=\rho u_xu_y,$$
$$M_{f7}^{eq}=\rho\left(T+u_y^2\right),\ M_{f8}^{eq}=\rho u_x\left[(D+I+2)T+u^2\right],\ M_{f9}^{eq}=\rho u_y\left[(D+I+2)T+u^2\right],$$
$$M_{f10}^{eq}=3\rho u_xT+\rho u_x^3,\ M_{f11}^{eq}=\rho u_yT+\rho u_x^2u_y,\ M_{f12}^{eq}=\rho u_xT+\rho u_xu_y^2,\ M_{f13}^{eq}=3\rho u_yT+\rho u_y^3,$$
$$M_{f14}^{eq}=\rho T\left[(D+I+2)T+u^2\right]+\rho u_x^2\left[(D+I+4)T+u^2\right],\ M_{f15}^{eq}=\rho u_xu_y\left[(D+I+4)T+u^2\right],$$
$$M_{f16}^{eq}=\rho T\left[(D+I+2)T+u^2\right]+\rho u_y^2\left[(D+I+4)T+u^2\right].$$

The elements of $\mathbf{M}_\mathbf{R}$ are

$$M_{R1}=0,\ M_{R2}=0,\ M_{R3}=0,\ M_{R4}=\rho(D+I)T',\ M_{R5}=\rho T',\ M_{R6}=0,\ M_{R7}=\rho T',$$
$$M_{R8}=(D+I+2)\rho u_xT',\ M_{R9}=(D+I+2)\rho u_yT',\ M_{R10}=3\rho u_xT',\ M_{R11}=\rho u_yT',$$
$$M_{R12}=\rho u_xT',\ M_{R13}=3\rho u_yT',\ M_{R14}=\rho\left[2T(D+I+2)+(D+I+5)u_x^2+u_y^2\right]T',$$
$$M_{R15}=\rho u_xu_y(D+I+4)T',\ M_{R16}=\rho\left[2T(D+I+2)+u_x^2+(D+I+5)u_y^2\right]T'.$$

REFERENCES

[1] C.A. Handley, B.D. Lambourn, N.J. Whitworth, et al, Understanding the shock and detonation response of high explosives at the continuum and meso scales, Appl. Phys. Rev. 5 (2018) 011303.

[2] W.E. Baker, P.A. Cox, J.J. Kulesz, et al., Explosion hazards and evaluation, Elsevier, Amsterdam, 1983.

[3] R.K. Eckhoff, Dust explosions in the process industries: identification, assessment and control of dust hazards, Elsevier, New York, 2003.

[4] Y.A. Nikolaev, A.A. Vasil'ev, B.Y. Ul'yanitskii, Gas detonation and its application in engineering and technologies. Combust. Explos. Shock Waves 39(4) (2003) 382-410.

[5] R. Zhou, D. Wu, J. Wang, Progress of continuously rotating detonation engines, Chin. J. Aeronaut. 29 (2016) 15-29.

[6] V.N. Gamezo, D. Desbordes, E.S. Oran, Two-dimensional reactive flow dynamics in cellular detonation waves, Shock Waves, 9 (1999) 11-17.

[7] E. Nagnibeda, E. Kustova, Nonequilibrium reacting gas flows: kinetic theory of transport and relaxation processes, Springer, Berlin, 2009.

[8] C.M. Romick, T.D. Aslam, J.M. Powers, The effect of diffusion on the dynamics of unsteady detonations, J. Fluid Mech., 699 (2012) 453-464.

[9] E.S. Oran, C.K. Oh, B.Z. Cybyk, Direct simulation Monte Carlo: recent advances and applications, Annu. Rev. Fluid Mech. 30 (1998) 403-441.

[10] S. Succi, The Lattice Boltzmann Equation for Fluid Dynamics and Beyond, Oxford University Press, New York, 2001.

[11] Y. Zhang, L. Zhu, R. Wang, et al., Discrete unified gas kinetic scheme for all Knudsen number flows. III. Binary gas mixtures of Maxwell molecules, Phys. Rev. E 97 (2018) 053306.

[12] C. Lin, K.H. Luo, L. Fei, et al., A multi-component discrete Boltzmann model for nonequilibrium reactive flows, Sci. Rep., 7 (2017) 14580.

[13] S. Succi, G. Bella, F. Papetti, Lattice kinetic theory for numerical combustion, J. Sci. Comput. 12 (1997) 395-408.

[14] O. Filippova, D. Haenel, A novel numerical scheme for reactive flows at low mach numbers, Comput. Phys. Commun. 129 (2000) 267-274.

[15] K. Yamamoto, N Takada, M. Misawa. Combustion simulation with Lattice Boltzmann method in a three-dimensional porous structure, Proc. Combust.Inst. 30 (2005) 1509-1515.

[16] S. Chen, J. Mi, H. Liu, C. Zheng, First and second thermodynamic-law analyses of hydrogen-air counter-flow diffusion combustion in various combustion modes, Int. J. Hydrogen Energy 37 (2012) 5234-5245.

[17] B. Yan, A. Xu, G. Zhang, et al., Lattice Boltzmann model for combustion and detonation, Front. Phys. 8 (2013) 94-110.

[18] A. Xu, C. Lin, G. Zhang, et al., Multiple-relaxation-time lattice Boltzmann kinetic model for combustion, Phys. Rev. E 91 (2015) 043306.

[19] C. Lin, A. Xu, G. Zhang, et al., Double-distribution-function discrete Boltzmann model for combustion, Combust. Flame 164 (2016) 137-151.

[20] C. Lin, K.H. Luo, MRT discrete Boltzmann method for compressible exothermic reactive flows, Comput. Fluids 166 (2018) 176-183.

[21] H.D. Ng, M.I. Radulescu, A.J. Higgins, et al., Numerical investigation of the instability for one-dimensional Chapman-Jouguet detonations with chain-branching kinetics, Combust. Theor. Model., 9 (2005) 385-401.

[22] H. Zhang, F. Zhuang, NND schemes and their applications to numerical simulation of two- and three-dimensional flows, Adv. Appl. Mech. 29 (1992) 193.

[23] P. Woodward, P. Colella, The numerical simulation of two-dimensional fluid flow with strong shocks, J. Comput. Phys. 54 (1984) 115.

[24] C. K. Law. Combustion physics, Cambridge University Press, Cambridge, 2006.